

# Superradiance and Exciton Delocalization in Perovskite Quantum Dot Superlattices

Daria D. Blach, Victoria A. Lumsargis, Daniel E. Clark, Chern Chuang, Kang Wang, Letian Dou, Richard D. Schaller, Jianshu Cao, Christina W. Li,\* and Libai Huang\*



Cite This: *Nano Lett.* 2022, 22, 7811–7818



Read Online

ACCESS |

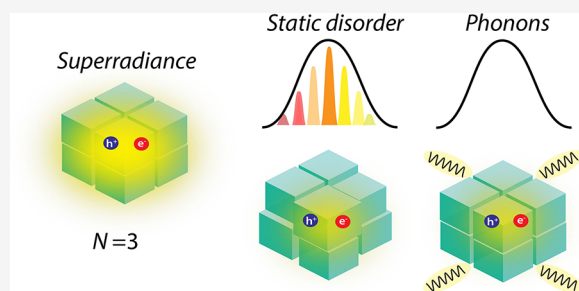
Metrics & More

Article Recommendations

Supporting Information

**ABSTRACT:** Achieving superradiance in solids is challenging due to fast dephasing processes from inherent disorder and thermal fluctuations. Perovskite quantum dots (QDs) are an exciting class of exciton emitters with large oscillator strength and high quantum efficiency, making them promising for solid-state superradiance. However, a thorough understanding of the competition between coherence and dephasing from phonon scattering and energetic disorder is currently unavailable. Here, we present an investigation of exciton coherence in perovskite QD solids using temperature-dependent photoluminescence line width and lifetime measurements. Our results demonstrate that excitons are coherently delocalized over 3 QDs at 11 K in superlattices leading to superradiant emission. Scattering from optical phonons leads to the loss of coherence and exciton localization to a single QD at temperatures above 100 K. At low temperatures, static disorder and defects limit exciton coherence. These results highlight the promise and challenge in achieving coherence in perovskite QD solids.

**KEYWORDS:** Quantum dot solids, superradiance, exciton coherence, perovskite



The realization of robust coherence in the solid state has been a long-standing challenge for quantum materials research. Superradiance, proposed by Dicke in 1954, describes a macroscopically coherent state that arises from the excitation of an ensemble of individual dipole emitters,<sup>1</sup> which is characterized by an accelerated radiative decay rate proportional to the number of emitters  $N$ . The realization of superradiance in solid-state systems is challenging due to inherent inhomogeneities and unavoidable fast dephasing processes.<sup>2–4</sup> Recently, colloidal metal halide perovskite quantum dots (QDs) have emerged as an exciting class of quantum emitters due to their near-unity quantum yields, large oscillator strengths, and long coherence times.<sup>5–13</sup> Superfluorescence, a many-body superradiance in which the transition dipole of many QDs self-lock into a macroscopic dipole after being photoexcited, has been recently reported in self-assembled perovskite QD superlattices (SLs).<sup>14,15</sup>

When inter-QD electronic coupling is larger than other dephasing fluctuations, a symmetric delocalized state is produced by the quantum superposition of all  $N$  possible single QD excitations. This delocalized state is superradiant because the transition dipole moment is enhanced by a factor of  $N$ , which is known as single-photon superradiance and difference from superfluorescence resulted from many-body effects.<sup>16</sup> Here, accelerated decay can be observed even if only one QD is excited. Such superradiance has been demonstrated in molecular aggregates with excitons delocalized over

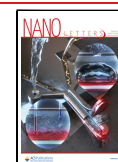
hundreds of molecules at low temperatures due to their strong electronic coupling (up to 200 meV).<sup>17–22</sup> Currently, a thorough understanding of the interplay between disorder and coherence in perovskite QD solids is lacking; such understanding is crucial for harnessing superradiance resulting from exciton delocalization to boost the performance of optoelectronic devices and engineer new quantum light sources. To address this question, we employed temperature-dependent and time-resolved photoluminescence (PL) spectroscopy to quantify exciton delocalization. We show that dipole coupling can outcompete disorder at low temperatures, resulting in single-photon superradiant radiative decay with a coherence number around 3 at 11 K for highly ordered SLs.

We employed highly ordered QD SLs with a small size distribution and well-defined inter-QD distance to probe the interplay between coherence and dephasing. Colloidal CsPbBr<sub>3</sub> QDs, whose absorbance and PL spectra are shown in Figure 1a (Figure S1 includes QD size distribution), were assembled into close-packed, three-dimensional (3D) micrometer-sized SLs on a silica substrate through slow evaporation (Figure S2).<sup>23</sup>

**Received:** June 18, 2022

**Revised:** August 28, 2022

**Published:** September 21, 2022



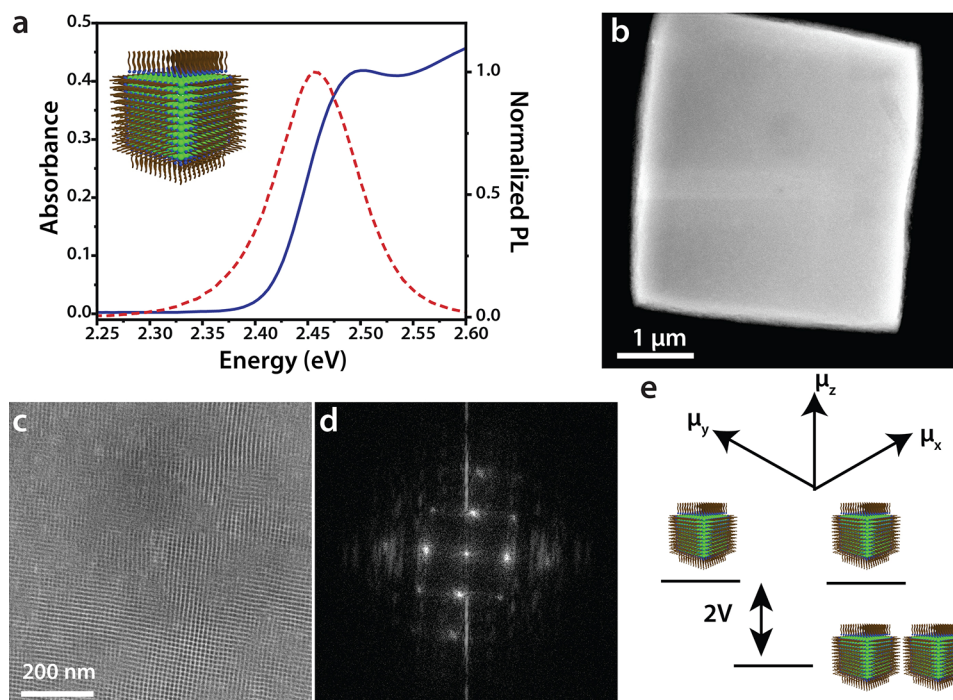


**Figure 1.** Structural and optical characterization of the CsPbBr<sub>3</sub> QD SLs. (a) Absorbance and PL spectra of CsPbBr<sub>3</sub> QDs in toluene. Inset: schematic illustration of a CsPbBr<sub>3</sub> QD capped with oleylamine and oleic acid. (b) Low-resolution HAADF-STEM image of a single SL. (c) High-resolution HAADF-STEM image of the same SL taken in the center showing ordered QD packing. (d) FFT of the high-resolution image. (e) Schematic of the nearest-neighbor dipole coupling between excitons with transition dipole  $\mu$  oriented in the  $x$ ,  $y$ , and  $z$  directions in a QD dimer.

To examine the ordering, high-angle annular dark-field scanning transmission electron microscopy (HAADF-STEM) images were collected on two representative SLs (Figures 1b,c and S3a,b). Cubic packing of QDs within the SL can be observed (Figure 1c). Fast Fourier transforms (FFT) of STEM images indicate long-range order within a given SL (Figures 1d and S3c). For the SL shown in Figure 1b,c, a well-defined spacing between the QDs ( $r$ ) is apparent. The first set of reflections occurs at 12 nm/c, a spacing that closely corresponds to the length of a 9 nm QD combined with a 3 nm spacing due to capping ligands.<sup>23</sup> In contrast, the SL shown in Figure S3a exhibits much greater disorder in the FFT as depicted in Figure S3c. A broad smear is observed from 10 to 14 nm/c, indicating substantial heterogeneity of  $r$  for the QD packing in this SL.

**Electronic Coupling.** Figure 1e illustrates the electronic coupling between excitons in CsPbBr<sub>3</sub> QDs due to dipole–dipole interaction. This static dipole interaction is valid for distances smaller than the emission wavelength. Radiative coupling, which is important at distances longer than the emission wavelength,<sup>24</sup> is neglected here and merits further investigation. For an isolated CsPbBr<sub>3</sub> QD, the lowest exciton state is a bright triplet with transition dipoles oriented in the  $x$ ,  $y$ , and  $z$  directions.<sup>12</sup> The nearest-neighbor dipole–dipole coupling is given by

$$V = \frac{\kappa\mu^2}{\epsilon R^3} \quad (1)$$

where  $\mu$  is the transition dipole,  $\kappa$  is the orientation factor,  $\epsilon$  is the dielectric constant, and  $R$  is the inter-QD distance. In dimers, the lowest state lies  $2V$  below the isolated QD transition.<sup>25</sup> In 3D SLs, exciton bands form due to periodic boundary conditions.<sup>26</sup> The lowest energy state at  $k = 0$  (zero

momentum, Brillouin zone center) is superradiant, which is the quantum superposition of all  $N$  possible single QD excitations. However, disorder can localize excitons by randomizing the relative frequency and phases. This scatters the population from the delocalized  $k = 0$  state to localized states with finite momentum, which leads to the destruction of coherence.<sup>19</sup>

We performed PL and reflectance spectroscopy over a wide temperature range (11–295 K) on multiple SLs grown on five different substrates, denoted as A, B, C, D, and E (Figure S4), to evaluate the degree of electronic coupling and disorder. Results from these SLs were compared to a thin film of highly dispersed QDs in a poly(methyl methacrylate) (PMMA) matrix, with mostly isolated QDs and small clusters (Figure S5a). The PL spectra for isolated QDs and the A1 SL are shown in Figures 2a and 2b, respectively (data for other SLs are shown in Figure S6). The center peak position and line width are compared for the isolated QDs and the A1 SL in Figure 2c,d (other SLs are presented in Figure S7). For the isolated QDs, the PL and reflectance (Figure S8) peak position red-shifts slightly as temperature decreases, which is mainly attributed to the reduced bandgap due to the decreased lattice constant at low temperatures.<sup>27</sup> While the center peak position for A1 and isolated QDs is similar between 100 and 295 K, the peak center of the SL further red-shifted from the isolated QDs below 100 K, with a shift of  $\sim 19$  meV at 11 K.

The red-shifted and narrower PL emission for the SLs at low temperatures is an optical signature of superradiance, where the collective excitonic states are shared by more than one QD. The energy shift is proportional to the effective dipole coupling strength  $V$ .<sup>28</sup> As detailed in the Supporting Information, we estimated  $V$  to be  $\sim 16$  meV, which is on the same order as the observed PL peak shift at 11 K and an order of magnitude higher than CdSe QD SLs.<sup>29</sup> Temperature-dependent

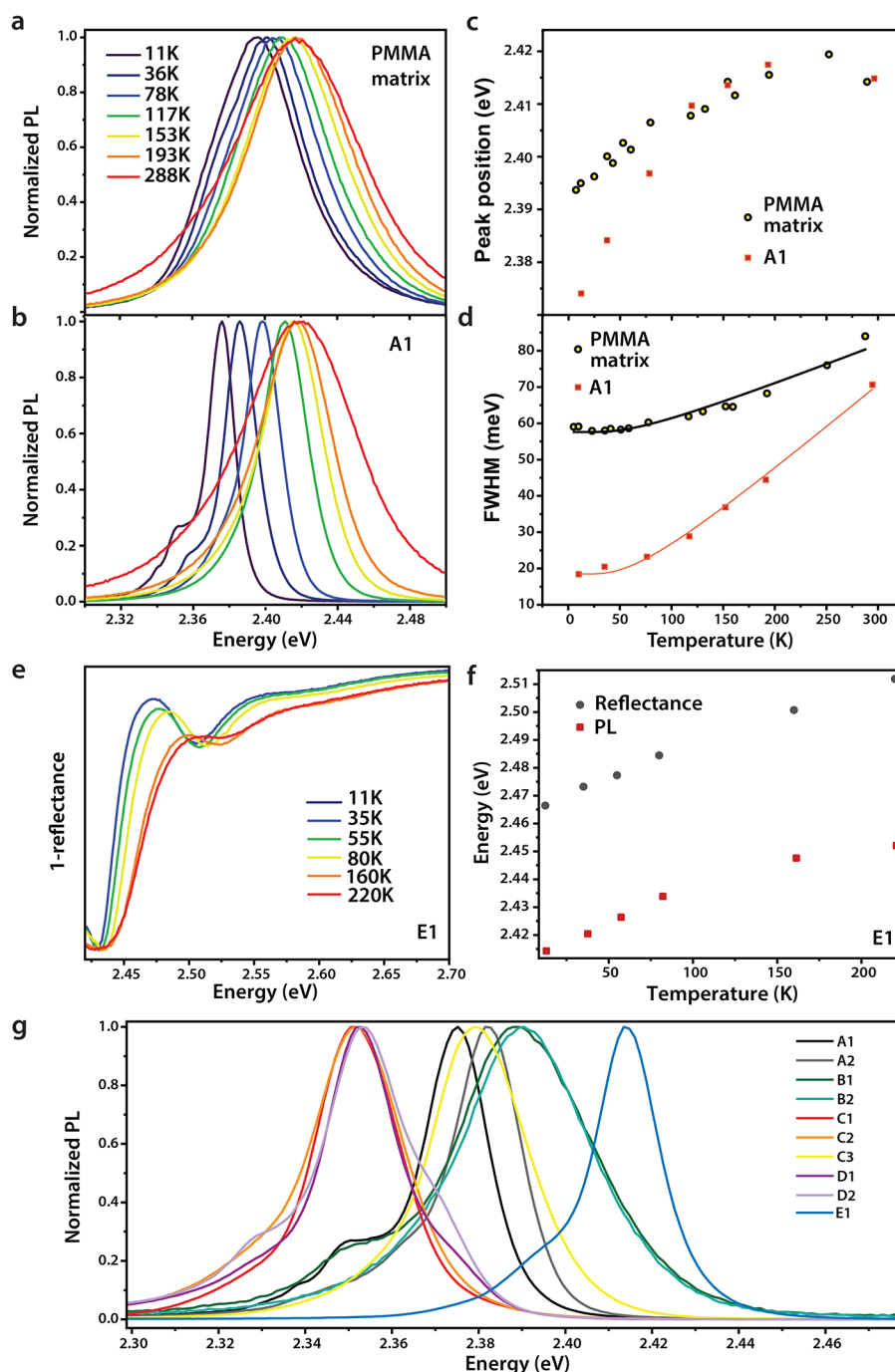


**Figure 2.** Temperature-dependent PL and reflectance spectroscopy to elucidate dynamic and static disorder. Temperature-dependent PL spectra acquired between 11 and 295 K for (a) isolated QDs and (b) the A1 SL. (c) Temperature-dependent center peak position extracted from PL spectra of isolated QDs and A1 SL. (d) Temperature-dependent FWHM extracted from PL spectra of isolated QDs and A1 SL. (e) Reflectance spectra for the E1 SL collected at temperatures between 11 and 220 K. (f) Temperature-dependent energy shift for reflectance and PL shown for E1 SL. (g) PL spectra of all SLs collected at 11 K.

reflectance spectra further confirm that red-shifted PL emission originated from the delocalized superradiant state. For the SL, we observed red-shifted exciton resonance with increased oscillator strength at low temperatures, consistent with superradiance (Figure 2e). In contrast, for isolated QDs, exciton absorption does not change significantly as a function of temperature (Figure S8). In addition, the energy gap between absorption and PL peak is constant across all temperatures in the SLs (Figure 2f), which validates that the red-shifted emission at low temperatures does not result from

other effects such as energy transfer from smaller to larger QDs. The larger red-shift at lower temperatures can be explained by how the transition dipole in isolated QDs increases due to the exciton size increasing.<sup>30,31</sup> Although the A, C, D, and E SLs examined here have different sizes and shapes (Figure S4), they have qualitatively similar behaviors. Therefore, we conclude that photonic effects do not play an important role.

**Phonon Scattering.** For both the SLs and isolated QDs, the PL line width becomes narrower at lower temperatures,



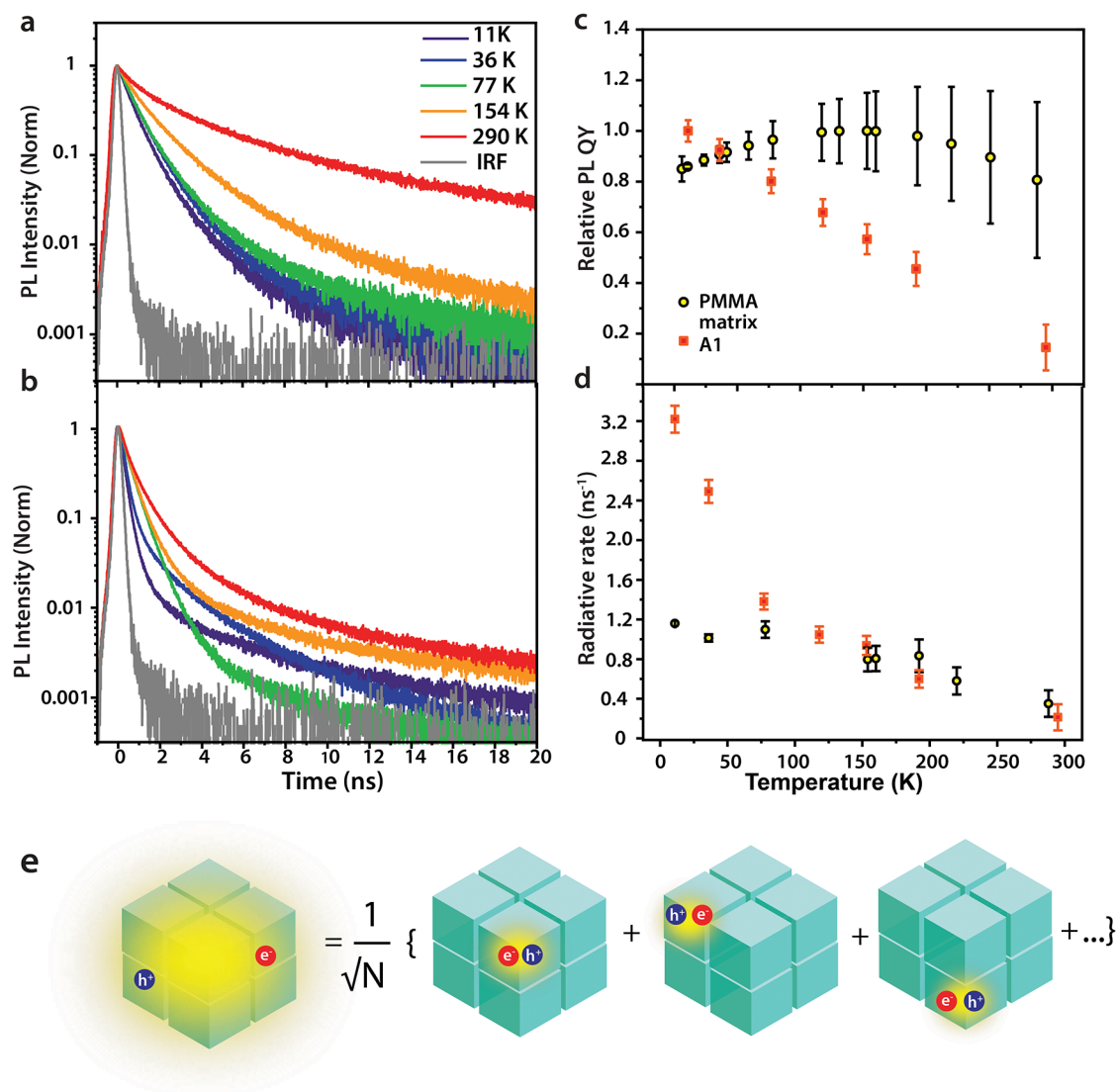


**Figure 3.** Superradiance enhanced radiative rates in SLs. Temperature-dependent PL lifetimes of (a) isolated QDs and (b) coupled QDs in A1 SL. (c) Temperature-dependent relative PLQY for isolated QDs and A1 SL. (d) Temperature-dependent radiative rates for isolated QDs and A1 SL. (e) Schematic illustration of the superradiant state produced by the quantum superposition of  $N$  single QD excitations.  $N = 3$  for the A1 SL.

consistent with the reduced dynamic disorder from phonon scattering.<sup>32</sup> From Figure 2d, we observe that for isolated QDs, the line width becomes constant below 100 K. In contrast, for some SLs, the line width continues to narrow below 100 K (data for A1 SL shown in Figure 2d, other SLs in Figure S7). This can be explained by exchange narrowing, where narrower line widths result from the averaging of inhomogeneities over many QD sites due to excitation delocalization at low temperatures.<sup>20</sup> Thus, the additional narrowing of the PL line width at low temperatures also confirms that excitons are delocalized over multiple QDs at low temperatures in some SLs.

Both acoustic and optical phonon scattering could contribute to the line width. We extracted the phonon scattering strength by fitting the temperature-dependent PL line width

$$\text{FWHM} = \Gamma_0 + \Gamma_{\text{AC}}T + \frac{\Gamma_{\text{LO}}}{e^{E_{\text{LO}}/k_{\text{B}}T} - 1} \quad (2)$$

where  $\Gamma_0$  is the inhomogeneous line width due to static disorder,  $\Gamma_{\text{AC}}$  ( $\Gamma_{\text{LO}}$ ) is the exciton longitudinal acoustic (optical) phonon coupling strength,  $E_{\text{LO}}$  is the energy of optical phonons,  $k_{\text{B}}$  is the Boltzmann distribution, and  $T$  is temperature.<sup>33–36</sup> We fixed  $E_{\text{LO}}$  to 16 meV corresponding to Pb–Br bending motions based on a previous work.<sup>37</sup> Fitting parameters are listed in Table S1. The  $\Gamma_{\text{LO}}$  values are similar for all SLs ( $\sim 40$  meV), indicating similar electron–phonon coupling strength. Overall, the coupling of optical phonons dominates the temperature-dependent line width, and the contribution from acoustic phonons is negligible, consistent with previous reports.<sup>38</sup>

**Static Disorder.** We use  $\Gamma_0$  as a measure of static disorder from inhomogeneities, and Figure 2g compares the PL spectra at 11 K. Static disorder has two main contributions: the size distribution of individual QDs that leads to different exciton energies and the inhomogeneities in the inter-QD distance resulting in fluctuations of QD-to-QD coupling. As shown in Figure 2g, all SLs have a narrower line width (17–35 meV) compared to isolated QDs (60 meV). The narrower line width indicates SLs have smaller static disorder, as expected from the

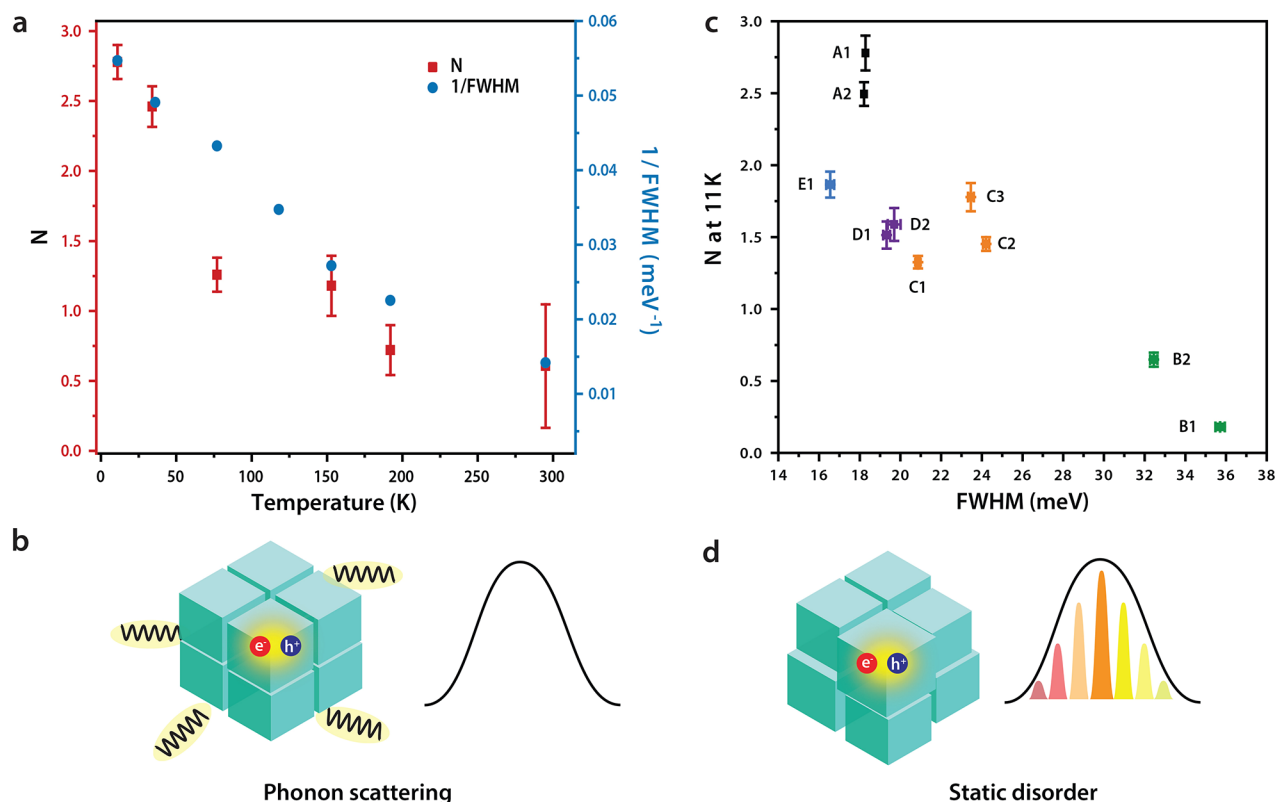


**Figure 4.** Phonon and disorder limited exciton superradiance. (a) Temperature dependence on  $N$  and the inverse of the FWHM for the A1 SL. (b) Diagram showing exciton localization due to phonon scattering at high temperatures. (c) Comparison of each SLs'  $N$  plotted against their respective FWHM at 11 K, showing the correlation between  $N$  and static disorder. (d) Schematic illustrating how static disorder leads to an inhomogeneously broadened line shape and exciton localization.

selection of a subpopulation of QDs with a smaller size distribution than the overall population through self-assembly. There are also variations in the PL line width between SLs, even when grown on the same substrate (e.g., C1, C2, and C3). A1 and E1 have the smallest FWHM ( $\sim 18$  meV), and B1 has the broadest FWHM (35 meV). Further examination of the PL spectra at 11 K in Figure 2g shows that some SLs have lower energy shoulder peaks. These are most likely caused by the existence of subdomains, composed of different sizes of QDs, within individual SLs.<sup>14,39</sup>

**Superradiance Enhanced Radiative Rate.** The redshifted and narrower PL emission of the SLs compared to isolated QDs at low temperature indicates that the exciton coherence length could extend beyond one QD. To determine the extent of delocalization, we compare the temperature-dependent PL decay of isolated QDs and the A1 SL in Figures 3a and 3b, respectively (Figure S9 includes other SLs' PL lifetimes). The averaged PL lifetime was determined by taking the  $1/e$  value of the dynamics curve. While the low-energy shoulder corresponding to subdomains with larger QDs could have slightly slower decay, energy transfer from smaller to larger QDs does not affect the extracted PL lifetime significantly (Figure S10), which could be explained by the radiative decay being faster than or comparable to the energy transfer time.<sup>40</sup> As the PL decay contains contributions from both radiative and nonradiative decay pathways, temperature-dependent PL quantum yields (PLQYs) were calculated, as shown in Figure 3c (calculation details are provided in the Supporting Information). The  $1/e$  lifetimes and PLQYs were used to calculate the radiative rates. For isolated QDs, the

absolute PLQY at 295 K was measured to be  $92 \pm 5\%$ . The PLQYs at different temperatures and in the SLs were determined relatively after correcting for temperature-dependent absorption.<sup>41</sup> The relative PLQYs of the isolated QDs and A1 SL are shown in Figure 3c (other SLs' PLQYs are included in Figure S11). The calculated temperature-dependent radiative rates for the isolated QDs and A1 SL are compared in Figure 3d (other SLs are shown in Figure S12). The uncertainties in the PLQYs and, consequently, radiative rates are largely due to heterogeneity (demonstrated in a PL intensity map of a representative SL in Figure S13). At room temperature, the PLQY values vary from SL to SL and are consistently lower than that of the isolated QDs, likely due to the increased probability of nonradiative energy transfer to defect sites in the SLs.<sup>42,43</sup> At low temperatures, the radiative rate in highly ordered SLs is enhanced by superradiance, which can outcompete nonradiative pathways and lead to PLQY close to 1.

Overall, the radiative rate increases as temperature decreases, as shown in Figure 3d for the A1 SL and isolated QDs (other SLs are included in Figure S12). Below 100 K, the radiative lifetime in the A1 SL becomes significantly shorter than the isolated QDs. At 11 K, the radiative rate in the A1 SL is  $3.2 \text{ ns}^{-1}$  compared to  $1.2 \text{ ns}^{-1}$  for the isolated QDs, which implies that the coherence length extends beyond one QD. In other words, superradiance is achieved when the transition dipole moment from multiple QDs merge into a single, large dipole (i.e.,  $N > 1$ ). We determined the average  $N$  by taking the ratio of the SL and isolated QD's radiative rates. On average, three QDs are coherently coupled at 11 K in the A1 SL. We note

that the radiative rate for the isolated QDs also increases from 0.4 to 1.2 ns<sup>-1</sup> as the temperature decreases from 298 to 11 K (Figure 3d). The enhanced radiative rate of isolated QDs at low temperatures can be explained by the increased exciton size, as phonon scattering is reduced.<sup>30,31</sup>

The superradiance observed here is different from previously reported superfluorescence.<sup>13,14</sup> For superfluorescence, many QDs are excited, and a burst of intense emission appears only above certain pump intensity thresholds after a time delay due to the time necessary for dipoles to become aligned by an external field.<sup>2</sup>  $N$  is dependent on how many QDs are excited and is varied with pump intensity. Here, the accelerated PL decay occurs at zero delay (also confirmed with a higher temporal resolution of ~25 ps, Figure S14) and is independent of pump intensity (Figure S15). We attribute this to single-photon superradiance,<sup>16</sup> where the quantum superposition of  $N$  single emitter excitations produces a symmetric superradiant state (schematically shown in Figure 3e). Such superradiance occurs even when the system interacts with one photon; therefore, all but one of the QDs are in the ground state. At high pump intensities, PL decay could become shorter due to exciton–exciton annihilation.<sup>44</sup>

$N$  shows a good correlation with the inverse of the PL line width as shown in Figure 4a, which implies that phonon scattering serves as the main mechanism for temperature-dependent decoherence (Figure 4b). The temperature dependence of  $N$  can be explained by exciton–phonon scattering creating a nonuniform, temperature-dependent population distribution of energy levels in momentum space  $k$ .<sup>18</sup> At lower temperatures, only the  $k = 0$  state is populated which corresponds to a coherence length extending over multiple QDs. Exciton–phonon scattering transfers oscillator strength from the  $k = 0$  state to other momentum states at high temperatures.<sup>18,45</sup> The spatial coherence length is restricted to a single QD as temperature increases above 100 K. In addition to phonon scattering, thermal averaging over superradiant and subradiant states could also reduce the coherence length and radiative rate at elevated temperatures.

Next, we discuss how static disorder and defects limit superradiance. SLs with narrower line width and lower static disorder showed faster radiative rates and a larger  $N$  (Figure 4c). The relationship between exciton localization and static disorder is illustrated in Figure 4d. While SLs in samples A, C, D, and E all display high radiative rates (1.5–3.2 ns<sup>-1</sup>) and relatively narrow FWHM (<25 meV) at 11 K, the radiative rates of the B SLs are much lower (0.2–0.8 ns<sup>-1</sup>) with broader FWHM (33–36 meV), corresponding to  $N$  values smaller than 1 at 11 K.  $N$  less than 1 indicates that the emission is subradiant (i.e., the exciton is localized to a coherent spatial extension smaller than the exciton in isolated QDs), which is likely due to defect-induced localized states, for example, from vacancies or dislocations in the lattices.<sup>46</sup> Figure S16 shows that over a broad temperature range,  $N$  for the B1 SL remains near or less than 1, suggesting the emission is dominated by localized excitons.

For C, D, and E SLs, the overall behavior is similar to the A SLs but with lower  $N$  (1.5–2 at 11 K). Larger static disorder in the C and D SLs can localize exciton wave functions by introducing random phase shifts, resulting in a smaller  $N$ . Another factor is defect-induced localized states, which are likely to be more prevalent in C, D, and E SLs than in A SLs. As shown in Figure S11, we observed a decrease in the relative PLQY for the C, D, and E SLs when the temperature is below

50 K. We did not observe this behavior in SL A1 (Figure 2c). This is likely due to some excitons being trapped in defect-induced localized states that lie below the superradiant bright state, which leads to a smaller  $N$ . We also compared results from a spun-cast film to that of the A1 SL (Figure S17). The FWHM and experimental lifetime at low temperatures for the spun-cast film fall between the isolated QDs and the SL due to aggregation likely occurring in the spun-cast film (Figure S5c,d). Exciton superradiance is not limited to SLs with long-range order but should also be possible in thin films with short-range order so long as electron coupling can outcompete disorder. For example, red-shifted and increased exciton absorption was observed recently at low temperatures in perovskite QD thin films.<sup>41,47</sup> Most recently, superfluorescence has also been reported in thin films of quasi-two-dimensional CsPbBr<sub>3</sub>.<sup>48</sup>

In conclusion, we reported the observation of superradiant decay from a delocalized exciton state with a coherence number of ~3 in SLs constructed from colloidal CsPbBr<sub>3</sub> QDs. Ultimately,  $N$  is determined by the competition between electronic coupling and disorder.<sup>17,18</sup> The large oscillator strength leads to electronic coupling between QDs with energies of ~16 meV. For the more ordered SLs, the electronic coupling can outcompete both static and dynamic disorder at low temperatures, leading to an average  $N$  of 3. It is not surprising that QDs in highly inhomogeneous environments, such as in the B SLs (static disorder >30 meV), would be unable to establish superradiance, as the energetic disorder is too great to allow the delocalization of excitons. These results suggest that further enhancement of coherence length requires increasing electronic coupling through tuning QD size and ligand design as well as improving materials' synthesis to decrease static disorder. The homogeneous line width at low temperatures for a single CsPbBr<sub>3</sub> QD has been reported to be ~80 μeV,<sup>32</sup> much smaller than the  $\Gamma_0$  at low temperature for the SLs here; thus, there is significant room to further reduce static disorder. For future studies, it will also be desirable to directly correlate structural disorder to coherence by performing high-resolution TEM and temperature-dependent optical spectroscopy measurements on the same SL.

## ■ ASSOCIATED CONTENT

### Supporting Information

The Supporting Information is available free of charge at <https://pubs.acs.org/doi/10.1021/acs.nanolett.2c02427>.

Experimental details, including synthesis of QDs, SLs, isolated QD PMMA film and spun-cast film, steady-state and time-resolved PL measurements; characterization of colloidal QD solutions, TEM and HAADF-STEM images of SLs; calculation of coupling strength, radiative rate and coherence number; supplemental figures (Figures S1–S17) including TEM of colloidal QDs, XRD spectrum, optical images of SLs, temperature-dependent PL and dynamics spectra of SLs and films, power-dependent dynamics spectra of a SL, temperature-dependent reflectance spectra of isolated QDs, PL intensity map of a SL; supplemental tables (Tables S1 and S2) for SLs' electron–phonon coupling strength and colloidal QDs' optical properties and sizes (PDF)



## AUTHOR INFORMATION

### Corresponding Authors

**Libai Huang** – Department of Chemistry, Purdue University, West Lafayette, Indiana 47907, United States; [orcid.org/0000-0001-9975-3624](https://orcid.org/0000-0001-9975-3624); Email: [libai-huang@purdue.edu](mailto:libai-huang@purdue.edu)

**Christina W. Li** – Department of Chemistry, Purdue University, West Lafayette, Indiana 47907, United States; [orcid.org/0000-0002-3538-9955](https://orcid.org/0000-0002-3538-9955); Email: [christinawli@purdue.edu](mailto:christinawli@purdue.edu)

### Authors

**Daria D. Blach** – Department of Chemistry, Purdue University, West Lafayette, Indiana 47907, United States

**Victoria A. Lumsargis** – Department of Chemistry, Purdue University, West Lafayette, Indiana 47907, United States; [orcid.org/0000-0001-9053-920X](https://orcid.org/0000-0001-9053-920X)

**Daniel E. Clark** – Department of Chemistry, Purdue University, West Lafayette, Indiana 47907, United States

**Chern Chuang** – Department of Chemistry, University of Toronto, Toronto, Ontario M5S 1A4, Canada

**Kang Wang** – Davidson School of Chemical Engineering, Purdue University, West Lafayette, Indiana 47907, United States

**Letian Dou** – Davidson School of Chemical Engineering, Purdue University, West Lafayette, Indiana 47907, United States; [orcid.org/0000-0001-6411-8591](https://orcid.org/0000-0001-6411-8591)

**Richard D. Schaller** – Department of Chemistry, Northwestern University, Evanston, Illinois 60208, United States; Center for Nanoscale Materials, Argonne National Laboratory, Lemont, Illinois 60439, United States

**Jianshu Cao** – Department of Chemistry, Massachusetts Institute of Technology, Cambridge, Massachusetts 02139, United States; [orcid.org/0000-0001-7616-7809](https://orcid.org/0000-0001-7616-7809)

Complete contact information is available at: <https://pubs.acs.org/10.1021/acs.nanolett.2c02427>

### Author Contributions

D.D.B., V.A.L., and D.E.C. contributed equally to this work.

### Notes

The authors declare no competing financial interest.

## ACKNOWLEDGMENTS

The work at Purdue was supported by the National Science Foundation through the Grant 2004339. The work was supported in part by the Research Instrumentation Center in the Department of Chemistry at Purdue University. Use of the Center for Nanoscale Materials, an Office of Science user facility, was supported by the U.S. Department of Energy, Office of Science, Office of Basic Energy Sciences, under Contract DE-AC02-06CH11357.

## REFERENCES

- (1) Dicke, R. H. Coherence in Spontaneous Radiation Processes. *Phys. Rev.* **1954**, *93*, 99–110.
- (2) Timothy Noe, G.; Li, Kim, J.-H.; Lee, J.; Wang, Y.; Wójcik, A. K.; McGill, S. A.; Reitze, D. H.; Belyanin, A. A.; Kono, J. Giant Superfluorescent Bursts from a Semiconductor Magneto-Plasma. *Nat. Phys.* **2012**, *8*, 219–224.
- (3) Fidler, H.; Wiersma, D. A. Collective Optical Response of Molecular Aggregates. *physica status solidi (b)* **1995**, *188*, 285–295.
- (4) Cong, K.; Zhang, Q.; Wang, Y.; Noe, G. T.; Belyanin, A.; Kono, J. Dicke Superradiance in Solids. *Journal of the Optical Society of America B* **2016**, *33*, C80.
- (5) Rainò, G.; Nedelcu, G.; Protesescu, L.; Bodnarchuk, M. I.; Kovalenko, M. V.; Mahrt, R. F.; Stöferle, T. Single Cesium Lead Halide Perovskite Nanocrystals at Low Temperature: Fast Single-Photon Emission, Reduced Blinking, and Exciton Fine Structure. *ACS Nano* **2016**, *10*, 2485–2490.
- (6) Jurow, M. J.; et al. Manipulating the Transition Dipole Moment of CsPbBr<sub>3</sub> Perovskite Nanocrystals for Superior Optical Properties. *Nano Lett.* **2019**, *19*, 2489–2496.
- (7) Koscher, B. A.; Swabeck, J. K.; Bronstein, N. D.; Alivisatos, A. P. Essentially Trap-Free CsPbBr<sub>3</sub> Colloidal Nanocrystals by Postsynthetic Thiocyanate Surface Treatment. *J. Am. Chem. Soc.* **2017**, *139*, 6566–6569.
- (8) Liu, F.; et al. Highly Luminescent Phase-Stable CsPbI<sub>3</sub> Perovskite Quantum Dots Achieving near 100% Absolute Photoluminescence Quantum Yield. *ACS Nano* **2017**, *11*, 10373–10383.
- (9) He, X.; Qiu, Y.; Yang, S. Fully-Inorganic Trihalide Perovskite Nanocrystals: A New Research Frontier of Optoelectronic Materials. *Adv. Mater.* **2017**, *29*, 1700775.
- (10) Protesescu, L.; Yakunin, S.; Bodnarchuk, M. I.; Krieg, F.; Caputo, R.; Hendon, C. H.; Yang, R. X.; Walsh, A.; Kovalenko, M. V. Nanocrystals of Cesium Lead Halide Perovskites (CsPbX<sub>3</sub>, X = Cl, Br, and I): Novel Optoelectronic Materials Showing Bright Emission with Wide Color Gamut. *Nano Lett.* **2015**, *15*, 3692–3696.
- (11) Utzat, H.; et al. Coherent Single-Photon Emission from Colloidal Lead Halide Perovskite Quantum Dots. *Science* **2019**, *363*, 1068–1072.
- (12) Becker, M. A.; et al. Bright Triplet Excitons in Caesium Lead Halide Perovskites. *Nature* **2018**, *553*, 189–193.
- (13) Rainò, G.; Utzat, H.; Bawendi, M. G.; Kovalenko, M. V. Superradiant Emission from Self-Assembled Light Emitters: From Molecules to Quantum Dots. *MRS Bull.* **2020**, *45*, 841–848.
- (14) Rainò, G.; Becker, M. A.; Bodnarchuk, M. I.; Mahrt, R. F.; Kovalenko, M. V.; Stöferle, T. Superfluorescence from Lead Halide Perovskite Quantum Dot Superlattices. *Nature* **2018**, *563*, 671–675.
- (15) Cherniukh, I.; et al. Perovskite-Type Superlattices from Lead Halide Perovskite Nanocubes. *Nature* **2021**, *593*, 535–542.
- (16) Röhlberger, R.; Schlage, K.; Sahoo, B.; Couet, S.; Ruffer, R. Collective Lamb Shift in Single-Photon Superradiance. *Science* **2010**, *328*, 1248–1251.
- (17) Spano, F. C.; Mukamel, S. Superradiance in Molecular Aggregates. *J. Chem. Phys.* **1989**, *91*, 683–700.
- (18) Spano, F. C.; Kuklinski, J. R.; Mukamel, S. Temperature-Dependent Superradiant Decay of Excitons in Small Aggregates. *Phys. Rev. Lett.* **1990**, *65*, 211–214.
- (19) Potma, E. O.; Wiersma, D. A. Exciton Superradiance in Aggregates: The Effect of Disorder, Higher Order Exciton-Phonon Coupling and Dimensionality. *J. Chem. Phys.* **1998**, *108*, 4894–4903.
- (20) Meinardi, F.; Cermignani, M.; Sassella, A.; Bonifacio, R.; Tubino, R. Superradiance in Molecular H Aggregates. *Phys. Rev. Lett.* **2003**, *91*, 247401.
- (21) Arias, D. H.; Stone, K. W.; Vlaming, S. M.; Walker, B. J.; Bawendi, M. G.; Silbey, R. J.; Bulović, V.; Nelson, K. A. Thermally-Limited Exciton Delocalization in Superradiant Molecular Aggregates. *J. Phys. Chem. B* **2013**, *117*, 4553–4559.
- (22) Doria, S.; et al. Photochemical Control of Exciton Superradiance in Light-Harvesting Nanotubes. *ACS Nano* **2018**, *12*, 4556–4564.
- (23) Krieg, F.; et al. Monodisperse Long-Chain Sulfofetate-Capped CsPbBr<sub>3</sub> Nanocrystals and Their Superfluorescent Assemblies. *ACS Central Science* **2021**, *7*, 135–144.
- (24) Coffey, B.; Friedberg, R. Effect of Short-Range Coulomb Interaction on Cooperative Spontaneous Emission. *PhRvA* **1978**, *17*, 1033–1048.
- (25) Teplakov, N. V.; Vovk, I. A.; Leonov, M. Y.; Baranov, A. V.; Fedorov, A. V.; Rukhlenko, I. D. Electronic and Optical Properties of Perovskite Quantum-Dot Dimer. *Semiconductors* **2019**, *53*, 2158–2161.
- (26) Vovk, I. A.; Teplakov, N. V.; Baimuratov, A. S.; Leonov, M. Y.; Baranov, A. V.; Fedorov, A. V.; Rukhlenko, I. D. Excitonic

Phenomena in Perovskite Quantum-Dot Supercrystals. *Phys. Chem. Chem. Phys.* **2018**, *20*, 25023–25030.

(27) Cheng, O. H.-C.; Qiao, T.; Sheldon, M.; Son, D. H. Size- and Temperature-Dependent Photoluminescence Spectra of Strongly Confined  $\text{CsPbBr}_3$  Quantum Dots. *Nanoscale* **2020**, *12*, 13113–13118.

(28) Chuang, C.; Cao, J. Universal Scalings in Two-Dimensional Anisotropic Dipolar Excitonic Systems. *Phys. Rev. Lett.* **2021**, *127*, 047402.

(29) Yoon, S. J.; Guo, Z.; dos Santos Claro, P. C.; Shevchenko, E. V.; Huang, L. Direct Imaging of Long-Range Exciton Transport in Quantum Dot Superlattices by Ultrafast Microscopy. *ACS Nano* **2016**, *10*, 7208–7215.

(30) p't Hooft, G. W.; van der Poel, W. A. J. A.; Molenkamp, L. W.; Foxon, C. T. Giant Oscillator Strength of Free Excitons in Gaas. *Phys. Rev. B* **1987**, *35*, 8281–8284.

(31) Feldmann, J.; Peter, G.; Göbel, E. O.; Dawson, P.; Moore, K.; Foxon, C.; Elliott, R. J. Linewidth Dependence of Radiative Exciton Lifetimes in Quantum Wells. *Phys. Rev. Lett.* **1987**, *59*, 2337–2340.

(32) Yu, B.; Zhang, C.; Chen, L.; Huang, X.; Qin, Z.; Wang, X.; Xiao, M. Exciton Linewidth Broadening Induced by Exciton-Phonon Interactions in  $\text{CsPbBr}_3$  Nanocrystals. *J. Chem. Phys.* **2021**, *154*, 214502.

(33) Lee, J.; Koteles, E. S.; Vassell, M. Luminescence Linewidths of Excitons in Gaas Quantum Wells Below 150 K. *Phys. Rev. B* **1986**, *33*, 5512.

(34) Fivaz, R.; Mooser, E. Electron-Phonon Interaction in Semiconducting Layer Structures. *Phys. Rev.* **1964**, *136*, A833–A836.

(35) Kaasbjerg, K.; Thygesen, K. S.; Jacobsen, K. W. Phonon-Limited Mobility in Single-Layer  $\text{MoS}_2$  from First Principles. *Phys. Rev. B* **2012**, *85*, 115317.

(36) Kim, S.; et al. High-Mobility and Low-Power Thin-Film Transistors Based on Multilayer  $\text{MoS}_2$  Crystals. *Nat. Commun.* **2012**, *3*, 1011.

(37) Ramade, J.; et al. Exciton-Phonon Coupling in a  $\text{CsPbBr}_3$  Single Nanocrystal. *Appl. Phys. Lett.* **2018**, *112*, 072104.

(38) Fu, M.; Tamarat, P.; Trebbia, J.-B.; Bodnarchuk, M. I.; Kovalenko, M. V.; Even, J.; Lounis, B. Unraveling Exciton-Phonon Coupling in Individual  $\text{FapbI}_3$  Nanocrystals Emitting near-Infrared Single Photons. *Nat. Commun.* **2018**, *9*, 3318.

(39) Mattiotti, F.; Kuno, M.; Borgonovi, F.; Jankó, B.; Celardo, G. L. Thermal Decoherence of Superradiance in Lead Halide Perovskite Nanocrystal Superlattices. *Nano Lett.* **2020**, *20*, 7382–7388.

(40) Enomoto, K.; Oizumi, R.; Aizawa, N.; Chiba, T.; Pu, Y.-J. Energy Transfer from Blue-Emitting  $\text{CsPbBr}_3$  Perovskite Nanocrystals to Green-Emitting  $\text{CsPbBr}_3$  Perovskite Nanocrystals. *J. Phys. Chem. C* **2021**, *125*, 19368–19373.

(41) Diroll, B. T.; Zhou, H.; Schaller, R. D. Low-Temperature Absorption, Photoluminescence, and Lifetime of  $\text{CsPbX}_3$  ( $X = \text{Cl}, \text{Br}, \text{I}$ ) Nanocrystals. *Adv. Funct. Mater.* **2018**, *28*, 1800945.

(42) Zhang, Z.; et al. Ultrafast Exciton Transport at Early Times in Quantum Dot Solids. *Nat. Mater.* **2022**, *21*, 533–539.

(43) Lapkin, D.; et al. Spatially Resolved Fluorescence of Caesium Lead Halide Perovskite Supercrystals Reveals Quasi-Atomic Behavior of Nanocrystals. *Nat. Commun.* **2022**, *13*, 892.

(44) Wei, K.; Zheng, X.; Cheng, X.; Shen, C.; Jiang, T. Observation of Ultrafast Exciton-Exciton Annihilation in  $\text{CsPbBr}_3$  Quantum Dots. *Adv. Opt. Mater.* **2016**, *4*, 1993–1997.

(45) Fidler, H.; Knoester, J.; Wiersma, D. A. Superradiant Emission and Optical Dephasing in J-Aggregates. *Chem. Phys. Lett.* **1990**, *171*, 529–536.

(46) van der Burgt, J. S.; et al. Cuboidal Supraparticles Self-Assembled from Cubic  $\text{CsPbBr}_3$  Perovskite Nanocrystals. *J. Phys. Chem. C* **2018**, *122*, 15706–15712.

(47) Shcherbakov-Wu, W.; Sercel, P. C.; Krieg, F.; Kovalenko, M. V.; Tisdale, W. A. Temperature-Independent Dielectric Constant in  $\text{CsPbBr}_3$  Nanocrystals Revealed by Linear Absorption Spectroscopy. *J. Phys. Chem. Lett.* **2021**, *12*, 8088–8095.

(48) Biliroglu, M.; et al. Room-Temperature Superfluorescence in Hybrid Perovskites and Its Origins. *Nat. Photonics* **2022**, *16*, 324–329.

## Recommended by ACS

### Acceleration of Biexciton Radiative Recombination at Low Temperature in $\text{CdSe}$ Nanoplatelets

Alexandra Brumberg, Richard D. Schaller, et al.

AUGUST 26, 2022  
NANO LETTERS

READ 

### Quantum Shells Boost the Optical Gain of Lasing Media

James Cassidy, Mikhail Zamkov, et al.

FEBRUARY 07, 2022  
ACS NANO

READ 

### Effects of Electronic Coupling on Bright and Dark Excitons in a 2D Array of Strongly Confined $\text{CsPbBr}_3$ Quantum Dots

Xueting Tang, Dong Hee Son, et al.

AUGUST 01, 2022  
CHEMISTRY OF MATERIALS

READ 

### Laser-Controlled Charge Transfer in a Two-Dimensional Organic/Inorganic Optical Coherent Nanojunction

Matheus Jacobs, Caterina Cocchi, et al.

MARCH 18, 2022  
ACS APPLIED NANO MATERIALS

READ 

Get More Suggestions >